Large-scale conductivity-tensor calculations for Hall effects in time-dependent wave-packet diffusion method

Hiroyuki Ishii,[1,2,*] Hiroyuki Tamura,[3] Masaru Tsukada,[3] Nobuhiko Kobayashi,[1] and Kenji Hirose[4]

[1]*Institute of Applied Physics and Tsukuba Research Center for Interdisciplinary Materials Science, University of Tsukuba, 1-1-1 Tennodai, Tsukuba, Ibaraki 305-8573, Japan*

[2]*JST-PRESTO, University of Tsukuba, 1-1-1 Tennodai, Tsukuba, Ibaraki 305-8573, Japan*

[3]*WPI-Advanced Institute for Materials Research, Tohoku University, 2-1-1 Katahira, Aoba-ku, Sendai 980-8577, Japan*

[4]*Smart Energy Research Laboratories, NEC Corporation, 34 Miyukigaoka, Tsukuba, Ibaraki 305-8501, Japan*

(Received 2 July 2014; revised manuscript received 7 October 2014; published 31 October 2014)

We present a computational methodology to evaluate the conductivity tensors of "large-scale" systems in a magnetic field based on the time-dependent wave-packet diffusion method. As demonstrations, we first apply the method to the two-dimensional square lattice model with static disorder and confirm appropriate magnetic-field dependence of conductivities from weak to strong magnetic-field regimes. Furthermore, we extend the method to apply to realistic systems and evaluate the influence of dynamical disorder on the Hall effects of organic semiconductors, taking microscopic molecular vibrations into account.

DOI: 10.1103/PhysRevB.90.155458 PACS number(s): 72.80.Le, 73.50.−h, 73.61.Ph, 73.43.−f

I. INTRODUCTION

The measurement of the Hall effect is an indispensable method in solid-state physics to find the carrier concentrations n, the sign of charge carriers q, and carrier mobilities μ of materials [1]. In fact, the Hall-effect measurements have been utilized for the characterizations of covalent-bond crystals, such as silicon semiconductors, and so on [2–4].

Recently, the understanding of charge transport properties of materials strongly modified by time-dependent structural changes, such as DNA and organic materials, has become a great scientific challenge. In the past, it was difficult to detect the Hall voltage of strongly disordered organic materials where the hopping transport is dominant because such uncorrelated hopping processes do not contribute to the Hall effect. A carrier produces the Hall voltage in a magnetic field and can be detected only when it holds in a coherent phase-correlated manner. Recently the fabrication of pure organic semiconductor single crystals with high mobility has become possible by the progress of synthesis technologies; as a result, experimental observations of Hall effects have been reported for the pentacene and rubrene single crystals [5–9]. The observed power-law temperature dependence of mobilities implies the bandlike transport, not the hopping transport [10–13]. It is expected that further advances of techniques on the pure crystallization will reveal the intrinsic transport properties of organic materials by eliminating the extrinsic static disorder.

As for the analysis of Hall effects, the simple semiclassical expression of the Hall coefficient $R_H = 1/qn$ is not sufficient at all due to the complicated shape of the electronic band structure and carrier scatterings in realistic materials. We must definitely go beyond the conventional free-electron treatment with energy-independent relaxation time to an alternative theoretical procedure of analysis with efficient computational approaches for the interpretations of Hall-effect measurements. In recent theoretical approaches to clarify the transport mechanism of materials strongly affected by time-dependent structural changes, the numerical simulation of wave-packet dynamics in dynamical structural disorder has been considered one of the most effective methods [14–18]. In our previous papers, we have reported the molecular vibration effects on the transport properties of organic semiconductors using the time-dependent wave-packet diffusion method [16,19,20]. However, the efficient theoretical treatment of Hall effects of organic materials has been missing.

In this paper, we present a methodology to evaluate the Hall effects of "large-scale" systems with the use of the quantum wave-packet dynamics. As demonstrations, we first apply the present method to the two-dimensional (2D) square lattice with the Anderson-type static disorder and confirm appropriate magnetic-field dependence of conductivities from the classical (weak magnetic field) to quantum (strong magnetic field) Hall-effect regimes. Furthermore, we extend the method to take the microscopic molecular vibration effects into account and evaluate the influence of dynamical disorder on the Hall effects of organic semiconductors.

II. METHODOLOGY

The electronic conductivities of metals and covalent semiconductors have frequently been treated by the semiclassical Boltzmann equation [21,22], whereas here we employ a purely quantum theory based on the Kubo formula on the real-space representation. We note that this method can also treat strongly disordered materials where the wave number is not a good quantum number. In our previous paper [23], we discussed the Hall effects using wave-packet dynamics in applied magnetic fields. However, since the evaluation of Hall conductivities requires time-consuming calculations of velocity-correlation functions $\langle \hat{v}_x(0)\hat{v}_y(t)\rangle$, the maximum system size was, in fact, restricted to $\sim 10^3$ sites and thus it was difficult to understand the Hall effects of materials by taking their microscopic crystal structures into account. Furthermore, the lower limit of magnetic-field strength is determined by the maximum system size because the cyclotron radius cannot become larger than the system size. This condition prevents us from

*ishii@bk.tsukuba.ac.jp

performing thorough quantitative evaluations of Hall effects from weak to strong magnetic-field regimes. To overcome these difficulties, we develop a computational approach to evaluate the conductivity tensor of large-scale systems.

Let us start to formulate the conductivity tensor of materials with the volume Ω based on the time-dependent form of the Kubo formula,

$$\sigma_{\zeta\xi} \equiv \frac{e^2}{\Omega}\int_0^{\beta} d\lambda \int_0^{+\infty} ds\ \mathrm{Tr}[\hat{\rho}(E_F)\hat{v}_{\xi}(0)\hat{v}_{\zeta}(s+i\hbar\lambda)], \quad (1)$$

where β is the inverse temperature $1/k_BT$, the density operator is defined as $\hat{\rho}(E_F) \equiv \exp\{(-\beta(\hat{H}-E_F)\}$, $\hat{v}_{\xi}(t) \equiv \hat{U}^{\dagger}(t)\hat{v}_{\xi}\hat{U}(t)$ is an electron velocity operator in the Heisenberg representation along the ξ direction, $i\hbar\hat{v}_{\xi} \equiv [\hat{H},\hat{\xi}]$, and $\hat{U}(t=N_t\Delta t) \equiv \Pi_{n=0}^{N_t-1}\exp\{i\hat{H}(n\Delta t)\Delta t/\hbar\}$ is the time-evolution operator. By introducing the modified density operator $\tilde{\rho}(E_F,u_{\xi}) \equiv \exp\{-\beta(\hat{H}-E_F-u_{\xi}\hat{v}_{\xi})\}$, the Kubo formula can be transformed into the following representation [24,25]:

$$\sigma_{\zeta\xi} = \lim_{t\to+\infty}\sigma_{\zeta\xi}(t), \quad (2)$$

$$\sigma_{\zeta\xi}(t) = \frac{e^2}{\Omega}\lim_{u_{\xi}\to 0}\int_0^t ds\ \frac{\partial}{\partial u_{\xi}}\mathrm{Tr}[\tilde{\rho}(E_F,u_{\xi})\hat{v}_{\zeta}(s)]. \quad (3)$$

This form has a great advantage for large-scale calculations, since we evaluate the average velocity using the modified density operator $\tilde{\rho}$, instead of time-consuming calculations of the velocity-correlation function in Eq. (1). Furthermore, to reduce the calculation cost, we compute the time-evolution operator numerically using the Chebyshev polynomials T_n and the Bessel functions J_n [14,16],

$$e^{i\frac{\hat{H}(t)}{\hbar}\Delta t} = \sum_{n=0}^{+\infty} e^{-i\frac{a\Delta t}{\hbar}} h_n i^n J_n\left(-\frac{b\Delta t}{\hbar}\right) T_n\left[\frac{\hat{H}(t)-a}{b}\right], \quad (4)$$

where the energy spectrum of $\hat{H}$ is included within the interval $[a-b,a+b]$, $h_0=1$ and $h_n=2$ $(n\geqslant 1)$. The Chebyshev polynomials obey the following recursive relation: $T_{n+1}(x) = 2xT_n(x) - T_{n-1}(x)$ with $T_0(x)=1$ and $T_1(x)=x$. When random-phase wave packets $|\Psi_n\rangle$ are employed as initial wave packets [26], Tr[·] of Eq. (3) can be evaluated effectively as follows:

$$\mathrm{Tr}[\tilde{\rho}(E_F,u_{\xi})\hat{v}_{\zeta}(s)] = \frac{N}{N_w}\sum_{n=1}^{N_w} e^{\beta E_F}\langle\Phi_n(s)|\hat{v}_{\zeta}|\Phi_n(s)\rangle, \quad (5)$$

where the Boltzmann-weighted random-phase wave packets at time s are defined by $|\Phi_n(s)\rangle \equiv \hat{U}(s)\exp\{-\frac{\beta}{2}(\hat{H}-u_{\xi}\hat{v}_{\xi})\}|\Psi_n\rangle$. The number of total sites and initial wave packets are represented by N and N_w, respectively. The use of random-phase wave packets, instead of the eigenvectors of the Hamiltonian, enables us to perform the order-N computation of conductivity tensor, suitable for the use of parallel computing.

Figure 1 shows the computing time and memory usage as a function of the number of sites N. The total number of time step is fixed at 10^3. We confirm that the order-N calculations with respect to both the computing time and the memory usage are realized for the system of up to 10^8 sites. The maximum system size corresponds to the 2D (one-layer) organic thin film

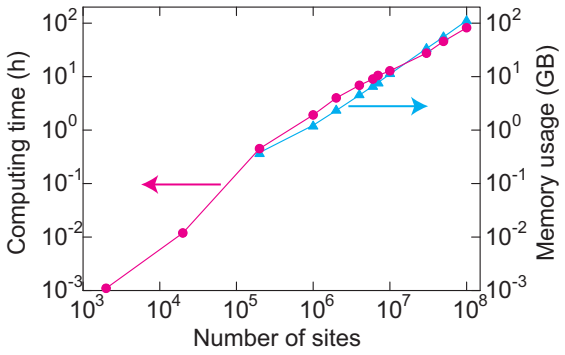

FIG. 1. (Color online) Computing time (red circles) and memory usage (blue triangles) per one initial wave packet as a function of site number of the 2D square lattice. The number of time step is set to 1000.

with each side length of a few micrometers. This shows that we can directly compute the transport properties of macroscopic materials with the realistic band dispersions from atomistic treatments. Furthermore, we can evaluate the Hall effects in realistic magnetic-field strengths from ∼1 T (tesla).

We consider that a magnetic field B is applied perpendicular to the 2D system on the xy plane and an electric current I_x flows along the x axis in an external electric field E_x. In this case, the Hall field E_y appears due to the transverse electromotive force. The Hall coefficient and Hall mobility are defined as follows:

$$R_H \equiv \frac{E_y}{I_xB} = \frac{\sigma_{xy}}{(\sigma_{xx}\sigma_{yy}+\sigma_{xy}^2)B}, \quad (6)$$

$$\mu_H \equiv -R_H\sigma, \quad (7)$$

where the conductivity $\sigma \equiv I_x/E_x$ in a magnetic field is given by $\sigma = (\sigma_{xx}\sigma_{yy}+\sigma_{xy}^2)/\sigma_{yy}$. The Hall factor γ_H is a dimensionless quantity defined by the ratio of the Hall mobility to the drift mobility,

$$\gamma_H \equiv \frac{\mu_H}{\mu}, \quad (8)$$

where the drift mobility is obtained from $\mu = \sigma/nq$. The drift mobility characterizes the transport along the direction of applied electric field E_x, while the Hall mobility characterizes the transport along the Hall field E_y.

Previous experimental researchers consider the Hall factor to be an indicator of whether or not the charge carrier shows the band transport properties [5–9]. Therefore, as demonstrations, we apply our alternative calculation method to two examples and evaluate the Hall factors.

III. RESULTS AND DISCUSSION

First, let us demonstrate how the present methodology is effective for the large-scale Hall-effect calculations. We consider the 2D square lattice of 1500 × 300 sites with a lattice constant $a = 5.0$ Å, where the periodic boundary condition is employed. The Hamiltonian is written by $\hat{H} = \sum_{ij}\gamma_{ij}\hat{c}_i^{\dagger}\hat{c}_j + \sum_i W_i\hat{c}_i^{\dagger}\hat{c}_i$. The magnetic-field effect is introduced into the

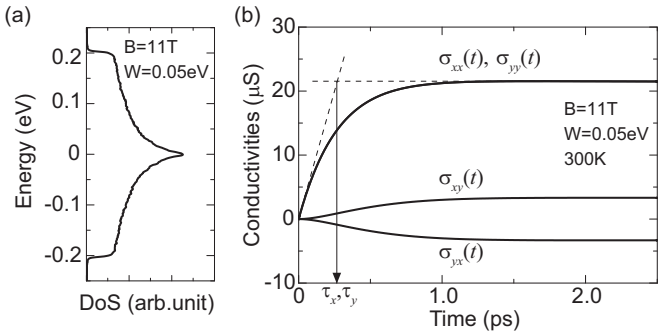

FIG. 2. (a) DoS of 2D square lattice with static disorder of $W = 0.05$ eV. (b) Time dependence of diagonal and Hall conductivities defined in Eq. (3) for the 2D square lattice with static disorder of $W = 0.05$ eV at 300 K. Magnitude of applied magnetic field is set at $B = 11$ T.

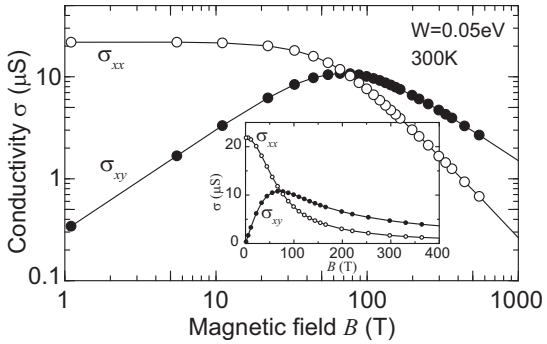

FIG. 3. Logarithmic plot of calculated diagonal and Hall conductivities of 2D square lattice with static disorder $W = 0.05$ eV at 300 K from weak to strong magnetic-field regime. Inset: Normal plot of conductivities as a function of magnetic-field strength.

Hamiltonian by multiplying the transfer energy γ_{ij}^0 by the phase factor $\gamma_{ij} = \gamma_{ij}^0 \exp\{i\frac{e}{\hbar}\int_{\mathbf{R}_i}^{\mathbf{R}_j} \mathbf{A}(\mathbf{r})d\mathbf{r}\}$, where $\mathbf{R}_i$ is the position vectors of the ith site [27] and $\mathbf{A}(\mathbf{r}) = (0, Bx, 0)$ is the vector potential for a magnetic field B. The transfer energy between nearest neighbors γ^0 is set to 0.05 eV, and thus the bandwidth is equal to 0.4 eV. The Anderson-type static disorder potential at the ith site is represented by W_i, which is selected randomly in the energy width $[-W/2, +W/2]$. Here, we introduce disorder potentials with a distribution of $W = 0.05$ eV. The charge concentration is fixed to 10^{12} cm^{-2}. The effective mass of square lattice is obtained as $m^* = \hbar^2/(2\gamma^0 a^2) = 2.78 \times 10^{-30}$ kg. When a magnetic field of 11 T is applied perpendicular to the square lattice, the energy distance between the nearest-neighbor Landau levels becomes $\hbar\omega_c = 0.42$ meV, where the cyclotron frequency is defined by $\omega_c = eB/m^*$. Since we introduce static disorder potentials, the Landau peaks in the density of states (DoS) are completely smeared by the disorder, as shown in Fig. 2(a). Here, the DoS is defined by $\nu(E) \equiv \mathrm{Tr}[\delta(E - \hat{H})]/\Omega$, where $\delta(x)$ is the Dirac's delta function.

Figure 2(b) shows the time-dependent conductivities obtained from Eq. (3) up to $t = 2.5$ ps at $B = 11$ T. We evaluate the conductivities using $N_w = 64$ different initial conditions with a time-step width of $\simeq$1 fs. We can confirm that the calculated time-dependent conductivities converge within the simulation time. The momentum relaxation time of charge carrier is evaluated as $\tau_x = 265$ fs from the intersection of two tangential lines with respect to $\sigma_{xx}(t)$ at $t = 0$ and $t \to +\infty$, as shown by two broken lines in Fig. 2(b). Since $\omega_c\tau = 0.17 \ll 1$ is satisfied in the present case, the classical Hall effect is obtained.

Then we change magnetic-field strengths from 1 to 500 T. Figure 3 shows the gradual transition from the weak magnetic-field (classical Hall-effect) regime to the strong magnetic-field (quantum Hall-effect) regime. We can confirm the typical B dependence of conductivities, i.e., $\sigma_{xx} \sim$ const and $\sigma_{xy} \propto B$ in the classical Hall-effect regime, while $\sigma_{xx} \propto 1/B^2 \to 0$ and $\sigma_{xy} \propto 1/B$ in the quantum Hall-effect regime. It appears that the boundary between the two regimes is located around $B =$ 70 T. In fact, the boundary condition between the two regimes is defined by $\omega_c\tau = 1$, which is satisfied with $B = 65.4$ T in the present case. The calculated Hall factor is $\gamma_H = 1.041$, which indicates $\mu \simeq \mu_H$, similar to the Hall factor of free-electron model. However, the obtained Hall factor reveals that the transport mechanism can not be completely understood by the ideal free-electron model. We confirm that the Anderson-type disorder creates localized states at the band edge due to the quantum interference. The diagonal conductivity slightly increases from 21.826 to 21.851 μS with increasing a magnetic field from 0 to 5.5 T because a magnetic field disturbs the quantum interference. Since the majority of states obeying the Fermi distribution at 300 K are extended (band) states, we can see subtle localization effects in the calculated conductivities. This result seems to be consistent with the calculated result of the free-electron-like Hall effect.

Next, we apply the present method to the transport properties of rubrene organic semiconductor single crystals and investigate the Hall effects. Recently, the Hall effects of rubrene single crystals have been observed in experiments [5,6]. The measured Hall effects show that the Hall mobility is nearly equal to the field-effect-transistor mobility around room temperature. This result is considered as evidence that the bandlike transport is realized in organic semiconductor single crystals [5–9]. We note that there are theoretical studies to show that transient localized states are produced by the strong thermal structural disorder and affect the transport properties [15,28,29]. Therefore, here we investigate the influence of intermolecular vibrations on the Hall effects of rubrene single crystals.

Figure 4(a) shows the herringbone packing structure of the rubrene single crystal. The material parameters, such as transfer energies, elastic constants, and electron-phonon (e-ph) coupling constants, are listed in Table I of Ref. [20]. We employ 1500×300 unit cells (900 000 molecules) to evaluate the transport properties. The calculated DoS of the highest occupied molecular orbital (HOMO) band is shown in Fig. 4(b), which is in good agreement with another theoretical study [30]. To describe the intermolecular vibration effects on charge transport properties, we compute the time evolution of electron wave packets combined with the molecular dynamics [20]. We introduce the time-dependent Hamiltonian for the charge carrier coupled with intermolecular vibrations, which is defined by $\hat{H}(t) = \sum_{ij} \gamma_{ij}(t)\hat{c}_i^\dagger \hat{c}_j$, where the time-dependent

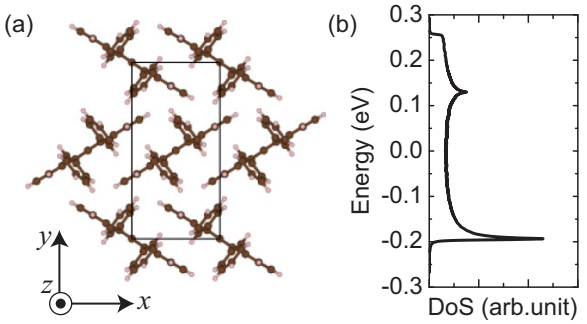

FIG. 4. (Color online) (a) Molecular packing structure of rubrene organic semiconductor single crystal. The rectangle represents the unit cell, whose size is 7.18×14.40 Å^2. (b) DoS of HOMO band of rubrene single crystal.

transfer energy is given by $\gamma_{ij}(t) = [\gamma_{ij}^0 + \alpha^{xy}\Delta R_{ij}(t) + \alpha^z \Delta Z_{ij}^2(t)] \exp\{i\frac{e}{\hbar}\int_{\mathbf{R}_i(t)}^{\mathbf{R}_j(t)} \mathbf{A}(\mathbf{r})d\mathbf{r}\}$. The bond-length modulations projected to the xy plane and to the z axis are represented by $\Delta R_{ij}(t)$ and $\Delta Z_{ij}(t)$, respectively. The transfer energy is well described by a linear function of bond-length change ΔR, while the change in transfer energy is given as a parabolic form with respect to ΔZ [20]. We evaluate the conductivities using $N_w = 448$ different initial conditions with a time-step width of $\simeq$1 fs. We confirm that the numerical error of time-step discretization is negligible. The classical Hamiltonian of the intermolecular vibrations is defined by $H = \sum_i (1/2)M\dot{\mathbf{R}}_i^2 + \sum_{i,j}(1/2)K_{ij}\Delta\mathbf{R}_{ij}^2 + \sum_i (1/2)K_z\Delta Z_i^2$, where M is the mass of a single molecule and K_{ij} represents the elastic constant. For simplicity, we assume the electrons (holes) do not affect the intermolecular vibrations. The motion of the nth molecule is given by the following equation: $M\ddot{\mathbf{R}}_n = -\sum_{ij} K_{ij}\Delta\mathbf{R}_{ij} - \sum_i K_z\Delta Z_i$. We fix the temperature by normalizing the kinetic energy of intermolecular vibrations at each time step.

We investigate the influence of intermolecular vibrations to the Hall effect of rubrene single crystals. To clarify the intrinsic charge transport properties, we introduce only the dynamical disorder induced by the intermolecular vibrations and exclude static disorder W. Figure 5(a) shows the time-dependent behavior of $\{\sigma_{\zeta\xi}(t)\}$ in a magnetic field $B = 5.3$ T at 300 K. Here, the charge concentration is fixed at 10^{12} cm^{-2}. The Hall conductivities $\sigma_{xy}(t)$ and $\sigma_{yx}(t)$ exhibit the same magnitude with opposite sign. We find the signature of transient localization of charge carriers in $\sigma_{xx}(t)$, which increases at short times in the ballistic transport regime and then shows a negative slope after taking the maximum value. The negative slope is a signal of the occurrence of backscattering underlying the phenomenon of localization [16,29]. On the other hand, the localization effect is not clearly seen in $\sigma_{yy}(t)$. In general, the strength of localization depends on the scattering rate $(1/\tau)$ because the frequent scatterings enhance the localization character. The calculated relaxation time τ_x is $\sim$100 fs, which is smaller than $\tau_y \sim 170$ fs and those of 2D square lattice discussed above. This is one of the reasons why the transient localization effect is only seen in $\sigma_{xx}(t)$ of rubrene crystal.

Figure 5(b) shows the conductivities as a function of temperature when we apply a magnetic field of 5.3 T. The obtained conductivities are monotonically decreasing with increasing temperature. The exponent n of T^{-n} dependence

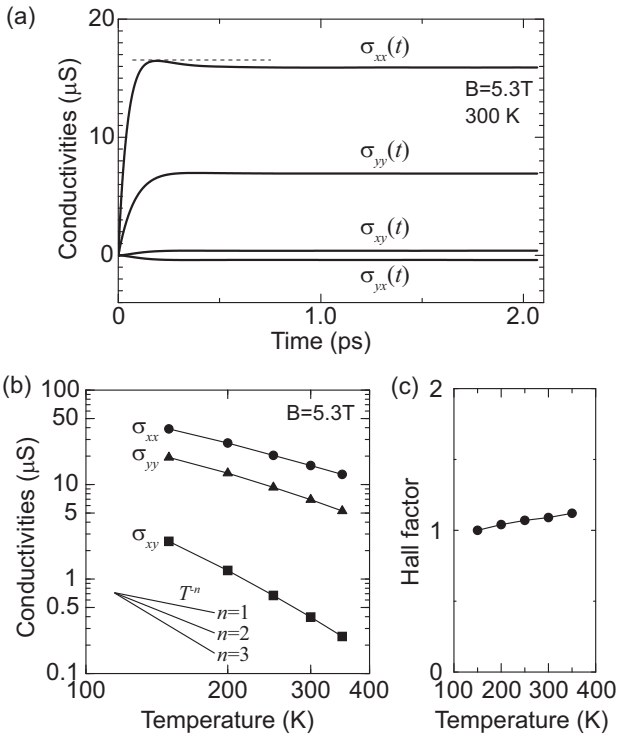

FIG. 5. (a) Time-dependent behaviors of conductivities of rubrene single crystal at 300 K. (b) Temperature dependence of conductivities σ_{xx}, σ_{yy}, and σ_{xy}. Magnitude of applied magnetic field is $B = 5.3$ T. (c) Hall factor $\gamma_H \equiv \mu_H/\mu$ as a function of temperature.

on σ_{xx} and σ_{yy} takes values from $n = 1$ to $n = 2$. There is a similarity between the present results and those by Troisi [15] and by Fratini and Ciuchi [28], who suggest that the exponent n of the temperature-dependent mobility lies between $n = 1$ and $n = 2$ due to the simultaneous presence of band states and transient localized states. The Hall conductivity σ_{xy} decreases more rapidly than the diagonal conductivities as the temperature increases. The exponent n of power-law temperature dependence lies between $n \simeq 2.5$ and 3.

From the calculated conductivities, we obtain the Hall factor as a function of temperature, as shown in Fig. 5(c). The obtained Hall factor becomes almost one with very weak temperature dependence. This shows that the intrinsic carrier mobility of rubrene single crystals is nearly equal to the Hall mobility, which is in good agreement with the recent Hall-effect measurements of rubrene single crystals [5,6], although the effects of transient localization on the Hall effects require further detailed investigations. From these calculations, we can say that the present simulation methodology provides an effective approach to clarify the unclear Hall effects of various soft and flexible materials strongly modified by time-dependent structural changes.

IV. SUMMARY

In summary, we present a computational methodology to evaluate the conductivity tensors of large-scale systems in a magnetic field based on the time-dependent wave-packet diffusion method. We first apply the method to the 2D square lattice model with static disorders and show appropriate magnetic-field dependence of conductivities in both weak and

strong magnetic-field regimes. We then extend the method to apply to the realistic systems of organic semiconductors. We study the influence of dynamical disorders on the Hall effects by taking microscopic molecular vibrations into account and find that the intrinsic carrier mobility of rubrene single crystals is nearly equal to the Hall mobility, in good agreement with recent experimental observations.

ACKNOWLEDGMENTS

We acknowledge J. Takeya, and T. Uemura for valuable suggestions. Financial support was provided by Japan Science and Technology Agency (JST)-PRESTO "Molecular technology and creation of new functions." Numerical calculations were performed at the Supercomputer Center, ISSP, University of Tokyo.

[1] S. M. Sze, *Semiconductor Devices: Physics and Technology*, 2nd ed. (Wiley, Hoboken, NJ, 2001).
[2] P. Norton, T. Braggins, and H. Levinstein, Phys. Rev. B **8**, 5632 (1973).
[3] A. Hackmann, D. Neubert, U. Scherz, and R. Schlief, Phys. Rev. B **24**, 4666 (1981).
[4] S. Madhavi, V. Venkataraman, J. C. Sturm, and Y. H. Xie, Phys. Rev. B **61**, 16807 (2000).
[5] J. Takeya, K. Tsukagoshi, Y. Aoyagi, T. Takenobu, and Y. Iwasa, Jpn. J. Appl. Phys. **44**, L1393 (2005).
[6] V. Podzorov, E. Menard, J. A. Rogers, and M. E. Gershenson, Phys. Rev. Lett. **95**, 226601 (2005).
[7] J.-F. Chang, T. Sakanoue, Y. Olivier, T. Uemura, M.-B. Dufourg-Madec, S. G. Yeates, J. Cornil, J. Takeya, A. Troisi, and H. Sirringhaus, Phys. Rev. Lett. **107**, 066601 (2011).
[8] T. Uemura, M. Yamagishi, J. Soeda, Y. Takatsuki, Y. Okada, Y. Nakazawa, and J. Takeya, Phys. Rev. B **85**, 035313 (2012).
[9] B. Lee, Y. Chen, D. Fu, H. T. Yi, K. Czelen, H. Najafov, and V. Podzorov, Nat. Mater. **12**, 1125 (2013).
[10] N. Karl, Synth. Met. **133**, 649 (2003).
[11] V. Podzorov, E. Menard, A. Borissov, V. Kiryukhin, J. A. Rogers, and M. E. Gershenson, Phys. Rev. Lett. **93**, 086602 (2004).
[12] Y. Okada, K. Sakai, T. Uemura, Y. Nakazawa, and J. Takeya, Phys. Rev. B **84**, 245308 (2011).
[13] N. A. Minder, S. Ono, Z. Chen, A. Facchetti, and A. F. Morpurgo, Adv. Mater. **24**, 503 (2012).
[14] S. Roche, J. Jiang, F. Triozon, and R. Saito, Phys. Rev. Lett. **95**, 076803 (2005).
[15] A. Troisi and G. Orlandi, Phys. Rev. Lett. **96**, 086601 (2006); J. Phys. Chem. A **110**, 4065 (2006).
[16] H. Ishii, N. Kobayashi, and K. Hirose, Appl. Phys. Express **1**, 123002 (2008); Phys. Rev. B **82**, 085435 (2010).
[17] J. Böhlin, M. Linares, and S. Stafström, Phys. Rev. B **83**, 085209 (2011).
[18] H. Tamura, M. Tsukada, H. Ishii, N. Kobayashi, and K. Hirose, Phys. Rev. B **86**, 035208 (2012).
[19] H. Ishii, K. Honma, N. Kobayashi, and K. Hirose, Phys. Rev. B **85**, 245206 (2012).
[20] H. Ishii, N. Kobayashi, and K. Hirose, Phys. Rev. B **88**, 205208 (2013).
[21] F. Szmulowicz, Phys. Rev. B **34**, 4031 (1986).
[22] Y. Fu, K. B. Joelsson, K. J. Grahn, W.-X. Ni, G. V. Hansson, and M. Willander, Phys. Rev. B **54**, 11317 (1996).
[23] H. Ishii, N. Kobayashi, and K. Hirose, Phys. Rev. B **83**, 233403 (2011).
[24] S. Fujita, *Statistical and Thermal Physics, Part II: Quantum Statistical Mechanics and Simple Applications* (Krieger, Malabar, FL, 1986).
[25] H. Tamura, M. Tsukada, H. Ishii, N. Kobayashi, and K. Hirose, Phys. Rev. B **87**, 155305 (2013).
[26] T. Markussen, R. Rurali, M. Brandbyge, and A.-P. Jauho, Phys. Rev. B **74**, 245313 (2006).
[27] Y. Hatsugai and M. Kohmoto, Phys. Rev. B **42**, 8282 (1990).
[28] S. Fratini and S. Ciuchi, Phys. Rev. Lett. **103**, 266601 (2009).
[29] S. Ciuchi, S. Fratini, and D. Mayou, Phys. Rev. B **83**, 081202(R) (2011).
[30] L. Tsetseris and S. T. Pantelides, Eur. Phys. J. Appl. Phys. **46**, 12511 (2009).